

CHOP: Counterfactual Human Preference Labels Improve Obstacle Avoidance in Visuomotor Navigation Policies

Gershom Seneviratne, Jianyu An, Vaibhav Shende, Sahire Ellahy, Yaxita Amin, Kondapi Manasanjani, Samarth Chopra, Jonathan Deepak Kannan, Dinesh Manocha
University of Maryland, College Park

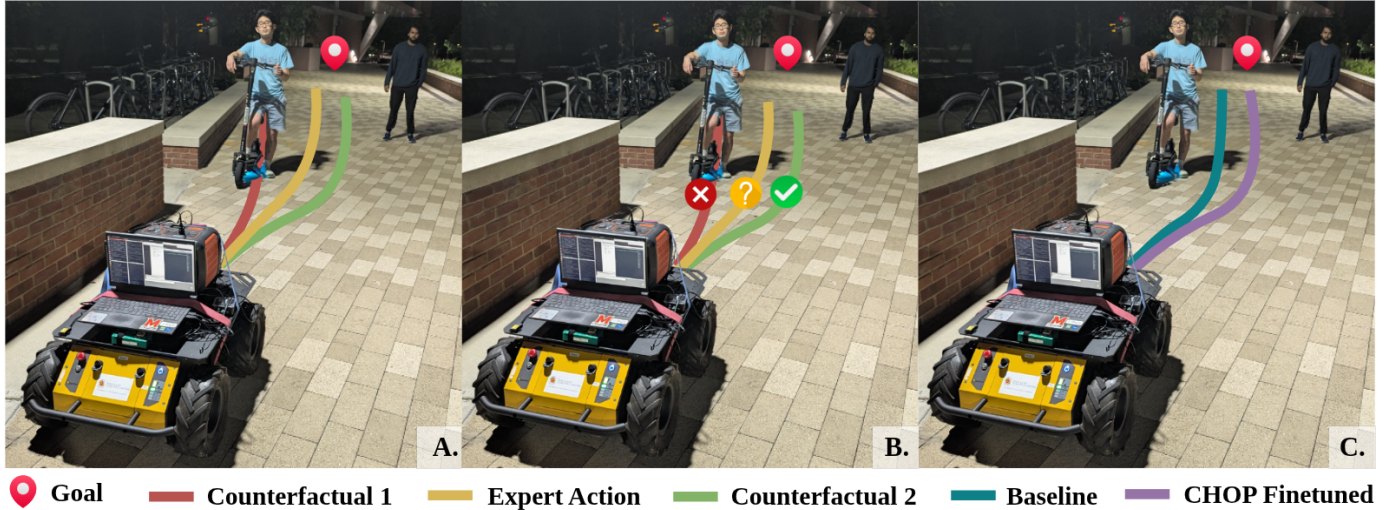


Fig. 1: CHOP: Counterfactual human preferences for obstacle avoidance and planning enable alignment of visuomotor navigation policies with human preference in ambiguous environments. (A) Given a single visual observation and goal, multiple distinct yet feasible navigation trajectories may exist. (B) Human annotators express preferences ($\checkmark > ? > \times$) over these counterfactual alternatives, capturing safety and contextual cues not explicitly observable, sometimes picking trajectories which are better than the operator action sequence. (C) CHOP aligns the policy to select the human-preferred trajectory, whereas the baseline policy selects a suboptimal path. Our method shows improvements in obstacle clearance, success rate, and average collision rate in real-world scenarios.

Abstract—Visuomotor navigation policies have shown strong perception–action coupling for embodied agents, yet they often struggle with safe navigation and dynamic obstacle avoidance in complex real-world environments. We introduce CHOP, a novel approach that leverages Counterfactual Human Preference Labels to align visuomotor navigation policies towards human intuition of safety and obstacle avoidance in navigation. In CHOP, for each visual observation, the robot’s executed trajectory is included among a set of counterfactual navigation trajectories: alternative trajectories the robot could have followed under identical conditions. Human annotators provide pairwise preference labels over these trajectories based on anticipated outcomes such as collision risk and path efficiency. These aggregated preferences are then used to fine-tune visuomotor navigation policies, aligning their behavior with human preferences in navigation. Experiments on the SCAND dataset show that visuomotor navigation policies fine-tuned with CHOP reduce near-collision events by 49.7%, decrease deviation from human-preferred trajectories by 45.0%, and increase average obstacle clearance by 19.8% on average across multiple state-of-the-art models, compared to their pretrained baselines. These improvements transfer to real-world deployments on a Ghost Robotics Vision60 quadruped, where CHOP-aligned policies improve average goal success rates by 24.4%, increase minimum obstacle clearance by 6.8%, reduce collision and intervention events by 45.7%, and improve normalized path completion by 38.6% on average across navigation scenarios, compared to their pretrained baselines. Our results highlight the value of counterfactual preference supervision in bridging the gap between large-scale visuomotor policies and human-aligned, safety-aware embodied navigation.

I. INTRODUCTION

For robots to be deployed at scale, navigation systems must be inexpensive, reliable, and robust across diverse environments. While LiDAR-based and stereo vision-based approaches can provide accurate geometric information, they are often expensive or unreliable in unstructured settings respectively [15, 23]. As a result, there has been growing interest in vision-based navigation, which relies only on onboard cameras and offers improved scalability and deployability. Recent advances in end-to-end visuomotor navigation, including architectures that operate on multimodal goal representations and the integration of large-scale models with generalist knowledge, have led to substantial progress in visual navigation [29, 27, 28, 13]. Despite this progress, vision-based navigation remains a central challenge in robotics, requiring agents to interpret complex visual scenes and make safe, goal-directed decisions in dynamic environments [19]. Most existing policies can achieve goal completion, but often do so at the cost of risky behaviors, such as approaching obstacles too closely or failing to account for dynamic agents [38, 34]. Typically, these offline navigation policies are trained to imitate trajectories from large-scale datasets, a natural approach due to the availability of large datasets. However, since these datasets are frequently collected via teleoperation, they inherently incorporate joystick noise, execution lag, and operator bias. This can

result in trajectories that, while safe, are suboptimal relative to other feasible paths under the same perceptual conditions. Consequently, policies trained on such data may inherit these inefficiencies, leading to the performance limitations observed in practice.

Addressing this limitation requires reasoning not only about the action that was taken, but also about what could have happened under alternative actions. Humans perform this effortlessly: when viewing a scene, we subconsciously evaluate multiple potential trajectories and favor those that minimize risk or social disruption. Such counterfactual reasoning, imagining the outcomes of unexecuted actions, is rarely incorporated into the training of current visuomotor navigation policies. Counterfactual trajectory supervision provides a natural way to address the aforementioned limitation, particularly in settings where the demonstrated trajectory may be safe but suboptimal relative to other feasible alternatives.

In this paper, we propose **CHOP** (**C**ounterfactual **H**uman preferences for **O**bstacle avoidance and **P**lanning), which instantiates counterfactual human preference supervision at scale via large-scale counterfactual preference data annotation, enabling the alignment of visuomotor policies with human preferences.

Main contributions: Our key contributions are summarized as follows:

- **Counterfactual human preference supervision for navigation:** We introduce counterfactual human preference supervision as a training signal for visuomotor navigation policy finetuning, enabling alignment toward human-preferred trajectories beyond imitation of demonstrated expert trajectories.
- **Large-scale counterfactual preference dataset:** We augment the **SCAND** [17] dataset with over one million counterfactual human preference pairs across multiple candidate trajectories per scene, providing a large-scale dataset of counterfactual trajectories which can be used to finetune visuomotor navigation policies. We use this dataset to finetune and evaluate state-of-the-art visuomotor and vision-language-action models against their baseline counterparts under safety and goal-oriented metrics.
- **Real-world validation:** We evaluate state-of-the-art visuomotor navigation policies and their CHOP-aligned counterparts through repeated real-world deployments on a Ghost Robotics Vision60 quadruped. We demonstrate consistent safety improvements in both offline and real-world evaluations, including a 49.7% reduction in near-collision events on SCAND and a 24.4% increase in real-world success rate on a quadruped robot. Our deployment uses an asynchronous plan-execute architecture that supports continuous policy inference, online trajectory updates, and modular swapping of visuomotor policies.
- **Open-source release:** We will release the **counterfactual preference dataset**, fine-tuned model weights, deployment and evaluation code to support future research on human-aligned, safety-aware visuomotor navigation policies.

Although counterfactuals have been explored in prior work as a data augmentation strategy for goal-reaching and instruction-following tasks [9], and as a source of cost for classical planners via inverse reinforcement learning [38], to the best of our knowledge, CHOP is the first large-scale counterfactual human preference dataset and method that leverages these preference labels as a direct supervision signal for aligning end-to-end visuomotor navigation policies with human preferences, enabling safer and more reliable navigation.

II. RELATED WORK

A. Vision-Based Navigation

Classical geometric planners such as the Dynamic Window Approach (DWA) [8] remain strong baselines for collision avoidance but depend on hand-crafted cost functions and typically rely on depth-based sensing, limiting their scalability for low-cost, vision-only robots. Early vision-based navigation research explored free-space and semantic segmentation techniques [12, 7, 11] for planning and obstacle awareness. Subsequent advances in topological memory representations [24, 3, 33] further improved visual navigation and inspired foundation-style models such as ViNT [29] and GNM [27], which train goal-conditioned, vision-based navigation policies across diverse robot datasets that generalize to a wide range of embodiments. Together, these developments reflect a broader shift from geometry-driven navigation toward data-driven, learning-based visual navigation.

Recent work has explored the use of large Vision-Language Models (VLMs) and Large Language Models (LLMs) to enhance embodied navigation. These approaches typically leverage pretrained VLMs or LLMs to interpret scene context, ground language instructions, infer navigational intent, and provide high-level semantic guidance to autonomous agents through multimodal prompts or natural-language feedback [31, 21, 35]. While such methods primarily focus on high-level semantic reasoning and instruction following, our work instead addresses safety alignment at the level of low-level visuomotor trajectory generation.

Building on this broader trend toward multimodal foundation models, recent visuomotor architectures take inspiration from Vision-Language-Action (VLA) models originally developed for robot manipulation [1, 39, 16]. VLAs jointly process visual inputs and language goals to produce low-level actions, coupling perception and semantics within a unified transformer backbone. Navigation-oriented extensions adopt this design for embodied movement, allowing policies to leverage language when available while functioning effectively as vision-based controllers [13, 2, 4]. Despite their broad generalization capabilities, existing visuomotor and VLA policies are typically trained to reproduce demonstrated trajectories, which are often collected via teleoperation and may reflect safe but suboptimal decisions due to execution noise or operator bias. As a result, such policies may inherit these limitations and produce goal-directed yet unsafe behavior in cluttered environments. In contrast, CHOP leverages human preferences

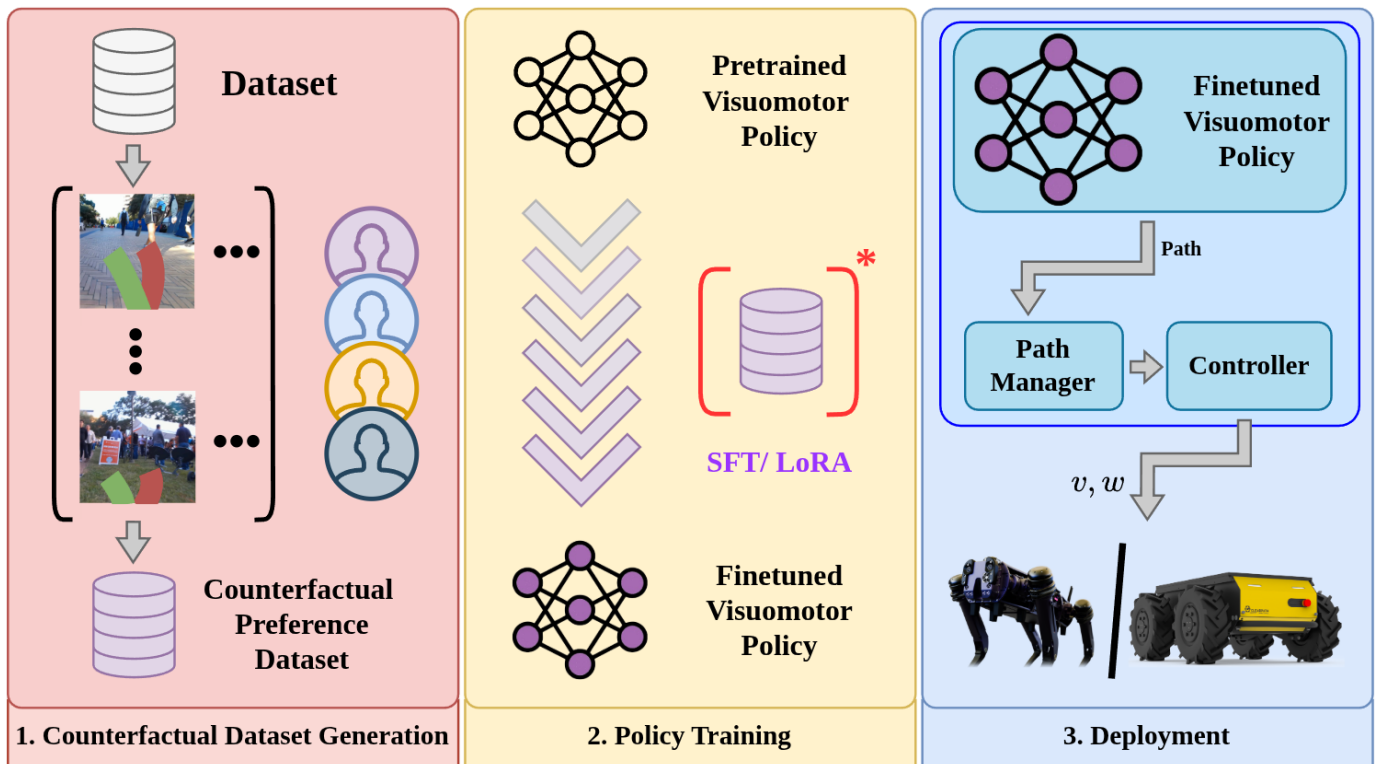


Fig. 2: Overview of CHOP. **(1) Counterfactual dataset generation:** Given a navigation dataset containing egocentric images and the trajectories executed by a robot, we generate multiple counterfactual trajectory alternatives for each observation. Human annotators provide binary preference labels over pairs of counterfactual trajectories, resulting in multiple comparisons per image (horizontal axis), while the process is repeated across the entire dataset (vertical axis). The aggregated preference annotations form the CHOP counterfactual preference dataset. **(2) Policy training:** For each observation, the dataset with the most preferred trajectory based on multiple preference labels for the same observation (*), is extracted from the binary rankings and used to fine-tune pretrained visuomotor navigation policies (e.g., OmniVLA [13], ViNT [29], GNM [27]) using Supervised Fine-Tuning (SFT) or Low Rank Adaptation (LoRA), producing a preference-aligned visuomotor policy. **(3) Deployment:** The resulting preference-aligned policies are deployed on real robot platforms, where predicted paths are executed by a downstream controller. Evaluations on both offline datasets and real-world robots demonstrate the benefits of counterfactual preference supervision for safer and more human aligned navigation.

over counterfactual trajectory alternatives to identify safer, more appropriate actions within identical visual scenes, and uses these human-preferred trajectories to align visuomotor policies toward safer navigation behavior.

B. Human Preference Alignment of Large Models

Human preference alignment has emerged as a central paradigm for steering large models toward human intent and safety, particularly in language and vision-language domains. A common approach is supervised fine-tuning (SFT) on human preference data [20, 6], often using parameter-efficient fine-tuning (PEFT) methods such as Low-Rank Adaptation (LoRA) [14], or reinforcement learning from human feedback (RLHF) [5, 22], where a learned reward model is optimized using methods such as Proximal Policy Optimization (PPO) [25].

In robotics and embodied AI, preference-based learning has been explored to align visuomotor policies with human intent, safety, and social norms [36, 5, 18, 10, 26]. These approaches typically rely on human feedback to train explicit reward models or to guide reinforcement learning, often requiring online interaction or iterative policy updates. In contrast, our work uses human preference encoded in counterfactual

trajectory pairs as a training signal to identify better trajectories than what’s available in the dataset, which can then be used to align visuomotor navigation policies using standard training pipelines without requiring online preference-based optimization.

III. BACKGROUND

In this section, we briefly review key formulations relevant to this work.

A. Visuomotor Navigation Policies

Visuomotor navigation policies[27, 29, 32, 26] learn an end-to-end mapping from sensory observations to control commands or short-horizon trajectories, optionally conditioned on a goal specification. Given a visual observation x_t and an optional goal representation g , the policy π_θ predicts a short-horizon action sequence:

$$\mathbf{a}_{t:t+K} = \pi_\theta(x_t, g), \quad (1)$$

where $\mathbf{a}_{t:t+K}$ denotes a sequence of actions or waypoints over a finite horizon K . Training is typically performed via

behavioral cloning to minimize an imitation loss

$$\mathcal{L}_{\text{BC}} = \|\mathbf{a}_{t:t+K} - \mathbf{a}_{t:t+K}^*\|_2^2, \quad (2)$$

where $\mathbf{a}_{t:t+K}^*$ denotes the expert action sequence or reference trajectory.

a) Navigation Vision-Language-Action (VLA) models.:

Vision-Language-Action (VLA) models for navigation [4, 13, 2] are a subclass of visuomotor navigation policies in which the goal representation g is specified in natural language. Given a visual observation x_t and a language instruction l , a VLA policy predicts a sequence of actions

$$\mathbf{a}_{t:t+K} = \pi_{\theta}(x_t, l), \quad (3)$$

where the language input conveys task intent or navigation goals. In practice, visual observations are encoded by a pretrained vision backbone and mapped into a shared representation space with language tokens via projection modules, allowing a unified policy network to condition low-level action generation on both visual and linguistic inputs.

B. Counterfactual Data for Models

Definition (Counterfactuals). A counterfactual refers to a hypothetical alternative to an observed event—answering the question, “what would have happened if conditions had been different?” Counterfactual reasoning is fundamental in causal inference and human decision-making, enabling one to compare actual outcomes with imagined alternatives that did not occur.

In the context of visuomotor navigation, a counterfactual represents an alternative feasible action sequence or short-horizon trajectory that could have been executed under identical perceptual conditions.

C. Preference Alignment

Preference alignment refers to methods for adapting a model’s behavior to reflect human preferences, typically expressed through comparisons or rankings of model outputs. Human preference data is commonly recorded in datasets and incorporated through either supervised fine-tuning[22], or reward-model-based alignment methods[37, 22].

a) Supervised Fine-Tuning (SFT): Supervised fine-tuning incorporates human preference annotations by converting them into supervised training targets. Given a set of candidate outputs for the same input, the human-preferred sample is treated as the positive example, and the model is fine-tuned to increase the likelihood of producing preferred outputs[22].

In practice, SFT can be performed either by updating all model parameters or through parameter-efficient fine-tuning methods such as LoRA [14, 30].

b) Reward-Model-Based Alignment: Reward-model-based alignment trains a scalar function $r_{\psi}(\cdot)$ to score candidate outputs according to human preferences. Given a pair of candidates with scores r_i and r_j , the

probability that i is preferred over j is commonly modeled using a Bradley–Terry formulation:

$$P(i \succ j) = \sigma(r_i - r_j), \quad (4)$$

where $\sigma(\cdot)$ denotes the logistic sigmoid. The reward model is trained by minimizing the negative log-likelihood of observed preference comparisons. Once trained, such reward models can be used for re-ranking policy alignment via reinforcement learning [22, 25].

These approaches represent two common paradigms for incorporating human preferences into model behavior. While both are applicable to aligning visuomotor navigation policies, CHOP instantiates one such paradigm as a proof of concept that counterfactual human preference labels can be used to improve navigation behavior, as described in Sec. IV.

IV. METHODOLOGY

Our goal is to align visuomotor navigation policies with human intuitions of safety using counterfactual preference supervision. Because standard navigation datasets contain only a single executed trajectory per observation and do not provide supervision over alternative feasible actions, CHOP first constructs a counterfactual preference dataset and then uses it as an offline training signal for policy alignment. As illustrated in Figure 2, the full training pipeline consists of three stages: (1) Counterfactual Preference Dataset Generation, (2) Policy Fine-tuning, and (3) Deployment in real-world scenarios. We describe each component below.

A. Counterfactual Preference Dataset Generation

1) Counterfactual Trajectory Generation: For each scene, we extract from the dataset a short-horizon trajectory of fixed length N , represented as a sequence of successive robot poses in the 2D plane,

$$\tau_0 = \{p_1, \dots, p_N\}, \quad (5)$$

where each waypoint $p_i = (x_i, y_i, \theta_i)$ denotes the robot’s planar position and orientation under a locally flat-ground assumption.

To construct meaningful counterfactual alternatives under identical perceptual conditions, we employ two complementary mechanisms: **(a) human-guided target annotation** and **(b) structured trajectory perturbations**.

a) Human-guided target annotation: Given the current egocentric camera image and a long-horizon navigation goal, annotators first indicate where the robot *should* head by clicking a target location in the image. A corresponding trajectory is generated by preserving the shape of the τ_0 (Eq. 5) and reparameterizing it to terminate at the clicked location, from which N waypoints are sampled along the resulting path. This trajectory is treated as one counterfactual candidate. During this same step, annotators may alternatively indicate that the robot should stop; this choice is encoded as a zero-motion trajectory of length N and included as an additional counterfactual candidate.



Fig. 3: Counterfactual trajectory generation and human preference annotation under identical egocentric observations. **A:** Trajectory recorded in the dataset. **B–C:** Structured counterfactual trajectories generated by rotating the executed trajectory counterclockwise and clockwise respectively. **D:** Human-guided target trajectory. **E:** Preference annotation interface, where annotators compare two overlaid trajectories and select the safer or more appropriate one. Trajectories are rendered in the robot’s egocentric frame; colors indicate different candidates and do not imply preference.

b) Structured trajectory perturbations.: To further populate the counterfactual set, we generate additional alternatives by rotating the trajectory recorded in the dataset (Eq. 5) about the robot’s ego frame. Specifically, we apply rotations sampled from a uniform distribution both clockwise and counterclockwise to the original trajectory, producing additional shape-preserving trajectories such that the total number of trajectories per observation is M .

The resulting trajectory set for each observation is

$$\mathcal{T}_{cf} = \{\tau_0, \tau_1, \dots, \tau_{M-1}\}, \quad (6)$$

For $i \neq 0$, τ_i denotes a counterfactual trajectory derived from annotator input and structured perturbations. Fig. 3

2) *Human Preference Annotation:* Each scene is represented by the egocentric camera image x_t . Annotators are shown x_t with two overlaid counterfactual trajectories (τ_i, τ_j) drawn from \mathcal{T}_{cf} and rendered in the robot’s egocentric frame. Because both trajectories are visualized on the same image, comparisons are made under identical perceptual conditions.

Annotators are asked to select the trajectory that is safer or more appropriate to execute, considering anticipated outcomes such as obstacle clearance, collision risk, and goal reaching. This yields a binary preference label

$$y_{ij} = \begin{cases} 1 & \text{if } \tau_i \text{ is preferred over } \tau_j, \\ 0 & \text{otherwise.} \end{cases}$$

For each scene with M counterfactual trajectories, pairwise comparisons induce $\binom{M}{2}$ binary preference annotations due to combinatorial pairing. The resulting preference dataset is

$$\mathcal{P} = \{(x_t, \tau_i, \tau_j, y_{ij})\}, \quad (7)$$

where $y_{ij} \in \{0, 1\}$ indicates whether trajectory τ_i is preferred over τ_j under observation x_t . The annotation interface used to collect these preferences is shown in Fig. 3.

3) *The CHOP Counterfactual Preference Dataset:* While standard navigation datasets provide only a single executed trajectory per observation, the CHOP dataset augments such data with human preferences over multiple feasible counterfactual

trajectories under identical perceptual input. We plan to release the full preference dataset to support reproducibility and future research. Summary statistics of the dataset are reported in Table I.

Number of annotated observations	187,920
Counterfactuals per observation (M)	4
Total counterfactual trajectories	751,680
Fraction where dataset trajectory is not preferred	70.51%
Total pairwise comparisons	1,127,520

TABLE I: Statistics of the CHOP preference dataset.

While our experiments instantiate CHOP by augmenting an existing navigation dataset [17] with human annotations, the same pipeline can be applied to other visuomotor datasets and can accommodate alternative preference sources, including vision–language models, without modification to the core procedure.

B. Preference-Based Fine-Tuning

As a proof of concept demonstrating the utility of counterfactual preference supervision, we use the collected preference annotations to align pretrained visuomotor navigation policies using supervised fine-tuning. For each scene, the annotated preference pairs (τ_i, τ_j, y_{ij}) over the counterfactual set \mathcal{T}_{cf} are aggregated to identify a single most preferred trajectory τ^* . Specifically, τ^* is selected as the trajectory that wins the largest number of pairwise comparisons. If multiple trajectories tie, we break ties deterministically by prioritizing annotator-suggested trajectories, followed by the trajectory recorded in the dataset; if neither is present among the tied candidates, one trajectory is selected uniformly at random.

Given an egocentric observation x_t and its corresponding preferred trajectory τ^* , a visuomotor policy π_θ predicts a trajectory $\hat{\tau} = \pi_\theta(x_t, g)$. The policy is then aligned by minimizing a supervised imitation loss between the predicted and preferred trajectories:

$$\mathcal{L}_{\text{align}} = \|\hat{\tau} - \tau^*\|_2^2. \quad (8)$$

For large pretrained models, we use parameter-efficient fine-tuning via LoRA [14] to adapt the policy while keeping the backbone frozen. Smaller models are fine-tuned end-to-end.

Although this best-trajectory distillation represents a simple instantiation of preference-based alignment, it serves to demonstrate that counterfactual human preferences provide an effective training signal for visuomotor policies. More general preference-learning paradigms—such as reward modeling or pairwise ranking objectives—are also compatible with the CHOP dataset and are left for future work.

C. Deployment in Real-World Scenarios

To deploy CHOP-aligned visuomotor policies on real robots, we use a lightweight and modular execution pipeline (Fig. 2) that decouples policy inference from trajectory execution. The policy runs asynchronously and periodically outputs a short-horizon trajectory, while a separate path management module maintains a consistent execution target by removing waypoints that the robot has already traversed and publishing a valid target waypoint. A simple tracking controller then follows this waypoint.

This design allows the robot to continue executing previously predicted trajectories while new predictions are computed, enabling robust online operation despite inference latency. Importantly, the execution pipeline is model-agnostic and can be used with any visuomotor policy that outputs a sequence of waypoints, allowing for modular swapping of navigation models without changes to the downstream execution stack.

V. ANALYSIS AND RESULTS

We evaluate the effectiveness of counterfactual preference alignment in improving safety-aware navigation across both large-scale offline datasets and real-world robot deployments. Our evaluation is designed to answer two key questions: (i) whether counterfactual human preference supervision improves obstacle-aware decision making under identical perceptual conditions, and (ii) whether these improvements transfer to real-world robotic navigation without degrading goal completion behavior.

A. Data Annotation Setup

All experiments use the CHOP counterfactual preference dataset described in Sec. IV-A. We generate $M = 4$ counterfactual trajectories per observation and use a fixed trajectory horizon of $N = 8$ waypoints. Preference annotations are collected from a pool of 8 human annotators, with each comparison presented under identical perceptual conditions. To reduce potential annotator bias, scenes for which counterfactual targets were provided by one set of annotators were assigned to a disjoint set of annotators for preference labeling, ensuring that annotators did not evaluate their own target selections.

Model	Near-Coll. ↓	Deviation ↓	Clearance ↑
OmniVLA (Base)	2453	0.6345	2.7647
OmniVLA + CHOP	897 (-63.4%)	0.3185 (-49.5%)	3.0332 (+9.7%)
ViNT (Base)	5192	1.8082	2.2472
ViNT + CHOP	3848 (-25.9%)	1.3216 (-26.9%)	2.5065 (+11.5%)
GNM (Base)	5529	1.9474	2.1629
GNM + CHOP	2219 (-59.7%)	0.8056 (-58.6%)	2.9887 (+38.1%)

TABLE II: Offline evaluation on SCAND. CHOP-aligned models demonstrate improved average obstacle clearance and reduced near-collision counts while reducing average deviation from the expert annotation for preferred trajectories.

B. Experimental Setup

We consider three state-of-the-art visuomotor navigation policies - OmniVLA [13], ViNT [29], and GNM [27] - as base models. Each model is evaluated in its original pretrained form and after fine-tuning using CHOP Counterfactual preference dataset. ViNT and GNM are fine-tuned end-to-end, while OmniVLA is fine-tuned using LoRA, updating only a small subset of policy parameters while keeping the visual backbone frozen.

For offline evaluation, we use the test split of the CHOP counterfactual preference dataset that is not seen by the models during fine-tuning. For real-world evaluation, we deploy both base and CHOP-aligned models on a Ghost Robotics Vision60 quadruped robot, running the policies on a laptop equipped with an NVIDIA RTX 5090 GPU and an Intel i9 processor.

C. Offline Evaluation on SCAND

We first evaluate policies offline using recorded sensor data from the test set of the SCAND dataset. For each frame, the policy predicts a short-horizon 2D trajectory conditioned on the egocentric camera observation and a sampled goal along the expert trajectory. Obstacle proximity is computed using synchronized 2D LiDAR scans by measuring the minimum Euclidean distance between interpolated trajectory points and observed obstacles.

We report the following metrics:

- **Near-Collision Count** : Count of trajectories with clearance below the width of the robot.
- **Average Trajectory Deviation from Preferred Trajectories (m)**: Average distance between the predicted trajectory and the annotator-informed preferred trajectory.
- **Average Minimum Obstacle Clearance (m)**: Average Minimum distance between the planned trajectory and any obstacle.

Table II summarizes results across all evaluated models. CHOP-aligned policies consistently maintain larger safety margins compared to their base counterparts, reducing near-collision events while preserving trajectory fidelity to expert demonstrations. Notably, improvements are observed under identical visual observations, indicating that gains stem from improved action selection rather than perception changes.

D. Real-World Robot Evaluation

To assess real-world transfer, we deploy both base and CHOP-aligned policies on mobile robots navigating cluttered

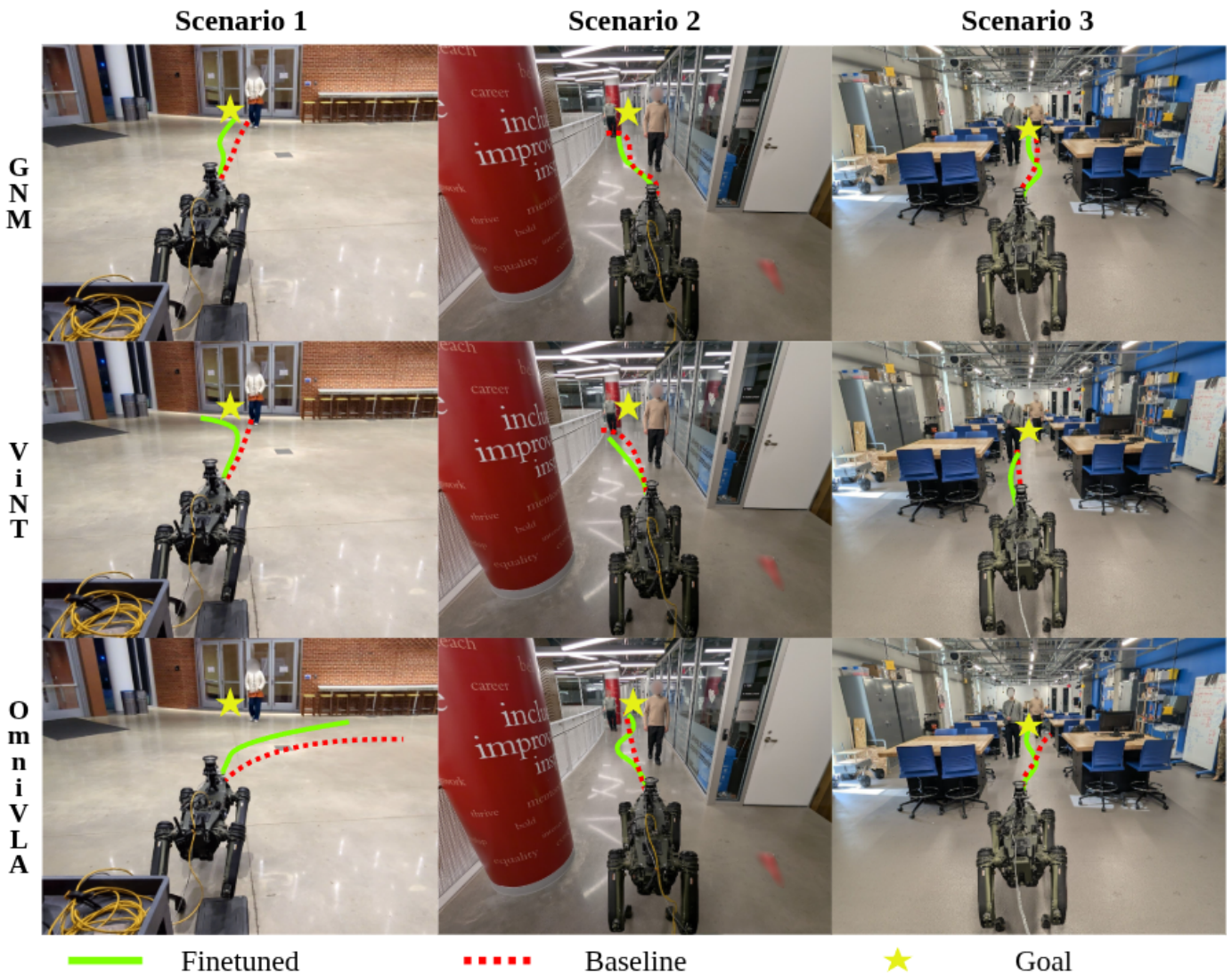


Fig. 4: Qualitative comparison of baseline and CHOP-finetuned visuomotor policies across three navigation scenarios, with rows corresponding to methods and columns corresponding to scenarios. Green trajectories denote CHOP-finetuned policies, while red dashed trajectories denote baseline behavior. GNM [27] and OmniVLA [13] exhibit improved obstacle avoidance and increased clearance after fine-tuning, whereas ViNT [29] shows more limited qualitative change.

environments with static and dynamic obstacles. (Fig. 4)

Scenario 1 - An open indoor space with the goal located straight ahead, with ample free space to the right and an exit corridor to the left. A person initially positioned near the goal walks towards the robot, requiring timely avoidance without excessive deviation from the goal. (Fig. 4 Column 1)

Scenario 2 - A constrained indoor corridor with glass walls on one side and structural pillars on the other, resulting in limited lateral clearance. People walk toward the robot from either side of the passageway, requiring the robot to anticipate motion, maintain safe distance from rigid obstacles, and execute precise avoidance maneuvers without drifting into the glass or pillars.(Fig. 4 Column 2)

Scenario 3 - A straight, narrow indoor passageway between rows of desks, with the goal located just beyond the

passageway. Two people emerge from opposite sides of the passageway and walk toward the robot in sequence. Due to the limited lateral clearance, the robot cannot proceed straight down the center and must shift to one side to avoid the first person, then quickly re-adjust to avoid the second. This scenario tests precise, anticipatory obstacle avoidance in tightly constrained spaces. (Fig. 4 Column 3)

We evaluate the following metrics in the real-world scenarios:

- **Success Rate (%)**: Percentage of runs that reach the goal within a predefined tolerance.
- **Average Minimum Obstacle Clearance (m)**: Average minimum distance between the robot and any obstacle along the executed trajectory, within the field of view of the camera. (calculated using LiDAR pointcloud converted to laserscan)
- **Average Number of Collisions**: Number of collision

Metrics	Model	Scenario 1	Scenario 2	Scenario 3
Success Rate (%) \uparrow	OmniVLA (Base)	0.0	80.0	0.0
	OmniVLA + CHOP	20.0	100.0	100.0
	ViNT (Base)	0.0	0.0	40.0
	ViNT + CHOP	0.0	0.0	20.0
	GNM (Base)	60.0	0.0	0.0
	GNM + CHOP	100.0	0.0	60.0
Average Min. Obstacle Clearance (m) \uparrow	OmniVLA (Base)	4.88	1.02	0.69
	OmniVLA + CHOP	4.73	1.29	0.85
	ViNT (Base)	4.19	0.98	0.64
	ViNT + CHOP	4.71	1.09	0.55
	GNM (Base)	4.24	1.11	0.71
	GNM + CHOP	4.57	1.07	0.83
Average Number of Collisions \downarrow	OmniVLA (Base)	0.0	0.2	2.0
	OmniVLA + CHOP	0.2	0.0	0.0
	ViNT (Base)	1.0	1.0	0.8
	ViNT + CHOP	0.0	1.8	1.2
	GNM (Base)	0.4	1.4	1.8
	GNM + CHOP	0.0	1.25	0.4
Normalized Path Completion \uparrow	OmniVLA (Base)	0.243	0.905	0.480
	OmniVLA + CHOP	0.469	1.000	1.000
	ViNT (Base)	0.359	0.625	0.650
	ViNT + CHOP	0.888	0.520	0.560
	GNM (Base)	0.803	0.360	0.412
	GNM + CHOP	1.000	0.463	0.803

TABLE III: Real-world evaluation across three navigation scenarios. CHOP-aligned models consistently improve safety-related metrics while preserving task success across diverse environments.

events, including physical contact or safety interventions. If intervention occurred to prevent contact with a dynamic obstacle, the event was counted as a collision, the obstacle was removed, and the run was allowed to continue.

- **Normalized Path Completion:** Fraction of the planned path completed toward the goal. Runs involving collisions yield values strictly less than 1.0 if terminated early.

All policies operate purely from onboard RGB observations, without access to depth or LiDAR during inference.

E. Discussion

In offline evaluations, we observe consistent improvements in obstacle clearance and stronger alignment with human preferences, as reflected by reductions in both near-collision events and the Deviation metric in Table II. These results indicate that CHOP fine-tuning successfully aligns visuomotor policies with the counterfactual preference supervision signal. Across architectures, OmniVLA and GNM benefit most from CHOP, exhibiting substantial reductions in near-collisions and deviation from human-preferred trajectories. In contrast, ViNT shows more limited gains, suggesting that its architecture or training dynamics may be less amenable to preference-based alignment under the same fine-tuning protocol.

We further evaluate CHOP-aligned models in three real-world scenarios (Table III). For OmniVLA and GNM, CHOP-aligned policies achieve higher success rates and improved path completion compared to their baselines, and make greater progress toward the goal with fewer collision events when the goal is not reached. For ViNT, success-rate improvements are less consistent; however, CHOP fine-tuning still improves obstacle clearance, indicating alignment toward safer trajectories.

Notably, in Scenarios 2 and 3, CHOP-aligned models occasionally exhibit stopping and waiting behaviors in response to tight dynamic obstacles that lead to collisions in the baseline models. These behaviors contribute to increased success

rates and reduced collision events and are likely introduced through counterfactual preference supervision. While teleoperated datasets such as SCAND contain very few explicit stopping behaviors in the recorded demonstrations, annotators frequently selected stopping as a preferred counterfactual action during CHOP annotation, particularly in crowded or ambiguous scenes. As a result, CHOP fine-tuning enables policies to internalize stopping and waiting as valid safety-oriented behaviors, even when such actions are underrepresented in the original training data.

A possible explanation for the comparatively weaker results observed for ViNT is that, while CHOP fine-tuning improves alignment with human preferences, it does not fundamentally alter the underlying capability of the base policy. As shown in Table III, the ViNT baseline already struggles in these scenarios prior to fine-tuning, suggesting that limitations in its base navigation behavior constrain the extent to which preference-based alignment can improve performance. Furthermore, the slight increase in the average number of collisions for OmniVLA in Scenario 1 can be attributed to improvements in normalized path completion, which often correspond to longer executed trajectories that increase exposure to dynamic obstacles and may introduce additional collision opportunities. While CHOP reduces the average number of collisions overall, increased path length can partially offset collision reductions in certain settings.

Overall, across both offline and real-world evaluations, counterfactual preference alignment improves safety-related behavior without degrading goal-reaching performance. In some scenarios, CHOP introduces safety-oriented behaviors, such as stopping and waiting, that are not explicitly present in the original datasets. These results suggest that human preference labels over counterfactual trajectories provide a powerful and complementary supervision signal to imitation learning, enabling visuomotor policies to internalize human notions of safe navigation beyond what is captured by trajectories present in datasets alone.

VI. CONCLUSION AND FUTURE WORK

We presented CHOP, a counterfactual preference supervision approach for aligning end-to-end vision-based visuomotor navigation policies with human preferences. By augmenting standard navigation datasets with human preferences over multiple feasible counterfactual trajectories evaluated under identical perceptual input, CHOP enables policies to learn from counterfactuals rather than treating demonstrated actions as inherently optimal.

Across large-scale offline evaluation and real-world robot deployments, CHOP-aligned policies consistently exhibit safer navigation behavior, including increased average obstacle clearance and reduced near-collision events, while preserving goal-reaching performance. These improvements generalize across multiple state-of-the-art visuomotor policies without requiring online human intervention or explicit safety constraints, demonstrating the effectiveness of counterfactual preference supervision as a scalable alignment signal.

While this work instantiates CHOP using best-trajectory distillation via supervised fine-tuning, the dataset naturally supports richer preference-learning paradigms such as reward modeling or pairwise ranking objectives. Exploring these alternatives is a promising direction for future work.

REFERENCES

- [1] Anthony Brohan, Noah Brown, Justice Carbajal, Yevgen Chebotar, Joseph Dabis, Chelsea Finn, Keerthana Gopalakrishnan, Karol Hausman, Alex Herzog, Jasmine Hsu, et al. Rt-1: Robotics transformer for real-world control at scale. *arXiv preprint arXiv:2212.06817*, 2022.
- [2] Mateo Guaman Castro, Sidharth Rajagopal, Daniel Gorbato, Matt Schmittle, Rohan Baijal, Octi Zhang, Rosario Scalise, Sidharth Talia, Emma Romig, Celso de Melo, et al. Vamos: A hierarchical vision-language-action model for capability-modulated and steerable navigation. *arXiv preprint arXiv:2510.20818*, 2025.
- [3] Devendra Singh Chaplot, Ruslan Salakhutdinov, Abhinav Gupta, and Saurabh Gupta. Neural topological slam for visual navigation. In *Proceedings of the IEEE/CVF conference on computer vision and pattern recognition*, pages 12875–12884, 2020.
- [4] An-Chieh Cheng, Yandong Ji, Zhaojing Yang, Zaitian Gongye, Xueyan Zou, Jan Kautz, Erdem Biyik, Hongxu Yin, Sifei Liu, and Xiaolong Wang. Navila: Legged robot vision-language-action model for navigation. *arXiv preprint arXiv:2412.04453*, 2024.
- [5] Paul F Christiano, Jan Leike, Tom Brown, Miljan Martic, Shane Legg, and Dario Amodei. Deep reinforcement learning from human preferences. *Advances in neural information processing systems*, 30, 2017.
- [6] Guanting Dong, Hongyi Yuan, Keming Lu, Chengpeng Li, Mingfeng Xue, Dayiheng Liu, Wei Wang, Zheng Yuan, Chang Zhou, and Jingren Zhou. How abilities in large language models are affected by supervised fine-tuning data composition. In *Proceedings of the 62nd Annual Meeting of the Association for Computational Linguistics (Volume 1: Long Papers)*, pages 177–198, 2024.
- [7] Rui Fan, Hengli Wang, Peide Cai, and Ming Liu. Sne-roadseg: Incorporating surface normal information into semantic segmentation for accurate freespace detection. In *European Conference on Computer Vision*, pages 340–356. Springer, 2020.
- [8] Dieter Fox, Wolfram Burgard, and Sebastian Thrun. The dynamic window approach to collision avoidance. *IEEE robotics & automation magazine*, 4(1):23–33, 2002.
- [9] Catherine Glossop, William Chen, Arjun Bhorkar, Dhruv Shah, and Sergey Levine. Cast: Counterfactual labels improve instruction following in vision-language-action models. *arXiv preprint arXiv:2508.13446*, 2025.
- [10] Matthew Gombolay. Human-robot alignment through interactivity and interpretability: Don’t assume a “spherical human”. In *Proceedings of the Thirty-Third International Joint Conference on Artificial Intelligence*, pages 8523–8528, 2024.
- [11] Tianrui Guan, Divya Kothandaraman, Rohan Chandra, Adarsh Jagan Sathyamoorthy, Kasun Weerakoon, and Dinesh Manocha. Ga-nav: Efficient terrain segmentation for robot navigation in unstructured outdoor environments. *IEEE Robotics and Automation Letters*, 7(3):8138–8145, 2022.
- [12] Noriaki Hirose, Amir Sadeghian, Marynel Vázquez, Patrick Goebel, and Silvio Savarese. Gonet: A semi-supervised deep learning approach for traversability estimation. In *2018 IEEE/RSJ international conference on intelligent robots and systems (IROS)*, pages 3044–3051. IEEE, 2018.
- [13] Noriaki Hirose, Catherine Glossop, Dhruv Shah, and Sergey Levine. Omnivla: An omni-modal vision-language-action model for robot navigation. *arXiv preprint arXiv:2509.19480*, 2025.
- [14] Edward J Hu, Yelong Shen, Phillip Wallis, Zeyuan Allen-Zhu, Yuanzhi Li, Shean Wang, Lu Wang, Weizhu Chen, et al. Lora: Low-rank adaptation of large language models. *ICLR*, 1(2):3, 2022.
- [15] Hochul Hwang, Soowan Yang, Jahir Sadik Monon, Nicholas A Giudice, Sunghoon Ivan Lee, Joydeep Biswas, and Donghyun Kim. Guidenav: User-informed development of a vision-only robotic navigation assistant for blind travelers. *arXiv preprint arXiv:2512.06147*, 2025.
- [16] Physical Intelligence, Kevin Black, Noah Brown, James Darpinian, Karan Dhabalia, Danny Driess, Adnan Esmail, Michael Equi, Chelsea Finn, Niccolo Fusai, et al. $\pi_{0.5}$: a vision-language-action model with open-world generalization. *arXiv preprint arXiv:2504.16054*, 2025.
- [17] Haresh Karnan, Anirudh Nair, Xuesu Xiao, Garrett Warrnell, Sören Pirk, Alexander Toshev, Justin Hart, Joydeep Biswas, and Peter Stone. Socially compliant navigation dataset (scand): A large-scale dataset of demonstrations for social navigation. *IEEE Robotics and Automation Letters*, 7(4):11807–11814, 2022.
- [18] Suzie Kim, Hye-Bin Shin, and Seong-Whan Lee. Aligning humans and robots via reinforcement learning from implicit human feedback. *arXiv preprint arXiv:2507.13171*, 2025.
- [19] Yu Liu, Shuting Wang, Yuanlong Xie, Tifan Xiong, and Mingyuan Wu. A review of sensing technologies for indoor autonomous mobile robots. *Sensors*, 24(4), 2024. ISSN 1424-8220. doi: 10.3390/s24041222. URL <https://www.mdpi.com/1424-8220/24/4/1222>.
- [20] Wei Lu, Rachel K Luu, and Markus J Buehler. Fine-tuning large language models for domain adaptation: Exploration of training strategies, scaling, model merging and synergistic capabilities. *npj Computational Materials*, 11(1):84, 2025.
- [21] Yao Mu, Qinglong Zhang, Mengkang Hu, Wenhai Wang, Mingyu Ding, Jun Jin, Bin Wang, Jifeng Dai, Yu Qiao, and Ping Luo. Embodiedgpt: Vision-language pre-

- training via embodied chain of thought. *Advances in Neural Information Processing Systems*, 36:25081–25094, 2023.
- [22] Long Ouyang, Jeffrey Wu, Xu Jiang, Diogo Almeida, Carroll Wainwright, Pamela Mishkin, Chong Zhang, Sandhini Agarwal, Katarina Slama, Alex Ray, John Schulman, Jacob Hilton, Fraser Kelton, Luke Miller, Maddie Simens, Amanda Askell, Peter Welinder, Paul F Christiano, Jan Leike, and Ryan Lowe. Training language models to follow instructions with human feedback. In S. Koyejo, S. Mohamed, A. Agarwal, D. Belgrave, K. Cho, and A. Oh, editors, *Advances in Neural Information Processing Systems*, volume 35, pages 27730–27744. Curran Associates, Inc., 2022. URL https://proceedings.neurips.cc/paper_files/paper/2022/file/b1efde53be364a73914f58805a001731-Paper-Conference.pdf.
- [23] Nitin J Sanket, Chahat Deep Singh, Varun Asthana, Cornelia Fermüller, and Yiannis Aloimonos. Morpheyes: Variable baseline stereo for quadrotor navigation. In *2021 IEEE International Conference on Robotics and Automation (ICRA)*, pages 413–419. IEEE, 2021.
- [24] Nikolay Savinov, Alexey Dosovitskiy, and Vladlen Koltun. Semi-parametric topological memory for navigation. *arXiv preprint arXiv:1803.00653*, 2018.
- [25] John Schulman, Filip Wolski, Prafulla Dhariwal, Alec Radford, and Oleg Klimov. Proximal policy optimization algorithms. *ArXiv*, abs/1707.06347, 2017. URL <https://api.semanticscholar.org/CorpusID:28695052>.
- [26] Gershon Seneviratne, Jianyu An, Sahire Ellahy, Kasun Weerakoon, Mohamed Bashir Elnoor, Jonathan Deepak Kannan, Amogha Thalihalla Sunil, and Dinesh Manocha. Halo: Human preference aligned offline reward learning for robot navigation. *arXiv preprint arXiv:2508.01539*, 2025.
- [27] Dhruv Shah, Ajay Sridhar, Arjun Bhorkar, Noriaki Hirose, and Sergey Levine. Gnm: A general navigation model to drive any robot. *arXiv preprint arXiv:2210.03370*, 2022.
- [28] Dhruv Shah, Błażej Osiański, Sergey Levine, et al. Lmnav: Robotic navigation with large pre-trained models of language, vision, and action. In *Conference on robot learning*, pages 492–504. PMLR, 2023.
- [29] Dhruv Shah, Ajay Sridhar, Nitish Dashora, Kyle Stachowicz, Kevin Black, Noriaki Hirose, and Sergey Levine. Vint: A foundation model for visual navigation. *arXiv preprint arXiv:2306.14846*, 2023.
- [30] Hakim Sidahmed, Samrat Phatale, Alex Hutcheson, Zhuonan Lin, Zhang Chen, Zac Yu, Jarvis Jin, Simral Chaudhary, Roman Komarytsia, Christiane Ahlheim, et al. Parameter efficient reinforcement learning from human feedback. *arXiv preprint arXiv:2403.10704*, 2024.
- [31] Daeun Song, Jing Liang, Amirreza Payandeh, Amir Hossein Raj, Xuesu Xiao, and Dinesh Manocha. Vlm-socialnav: Socially aware robot navigation through scoring using vision-language models. *IEEE Robotics and Automation Letters*, 2024.
- [32] Ajay Sridhar, Dhruv Shah, Catherine Glossop, and Sergey Levine. Nomad: Goal masked diffusion policies for navigation and exploration. In *2024 IEEE International Conference on Robotics and Automation (ICRA)*, pages 63–70. IEEE, 2024.
- [33] Asuto Taniguchi, Fumihito Sasaki, and Ryota Yamashina. Pose invariant topological memory for visual navigation. In *Proceedings of the IEEE/CVF International Conference on Computer Vision*, pages 15384–15393, 2021.
- [34] Junhui Wang, Dongjie Huo, Zehui Xu, Yongliang Shi, Yimin Yan, Yuanxin Wang, Chao Gao, Yan Qiao, and Guyue Zhou. Openbench: A new benchmark and baseline for semantic navigation in smart logistics. *arXiv preprint arXiv:2502.09238*, 2025.
- [35] Kasun Weerakoon, Mohamed Elnoor, Gershon Seneviratne, Vignesh Rajagopal, Senthil Hariharan Arul, Jing Liang, Mohamed Khalid M Jaffar, and Dinesh Manocha. Behav: Behavioral rule guided autonomy using vlms for robot navigation in outdoor scenes. In *2025 IEEE International Conference on Robotics and Automation (ICRA)*, pages 7044–7051. IEEE, 2025.
- [36] Christian Wirth, Riad Akrou, Gerhard Neumann, and Johannes Fürnkranz. A survey of preference-based reinforcement learning methods. *J. Mach. Learn. Res.*, 18:136:1–136:46, 2017. URL <https://api.semanticscholar.org/CorpusID:703818>.
- [37] Hongyi Yuan, Zheng Yuan, Chuanqi Tan, Wei Wang, Songfang Huang, and Fei Huang. Rrhf: Rank responses to align language models with human feedback. *Advances in Neural Information Processing Systems*, 36: 10935–10950, 2023.
- [38] Arthur Zhang, Harshit Sikchi, Amy Zhang, and Joydeep Biswas. Creste: Scalable mapless navigation with internet scale priors and counterfactual guidance. *arXiv preprint arXiv:2503.03921*, 2025.
- [39] Brianna Zitkovich, Tianhe Yu, Sichun Xu, Peng Xu, Ted Xiao, Fei Xia, Jialin Wu, Paul Wohlhart, Stefan Welker, Ayzaan Wahid, et al. Rt-2: Vision-language-action models transfer web knowledge to robotic control. In *Conference on Robot Learning*, pages 2165–2183. PMLR, 2023.

A. Dataset Split

For annotation and fine-tuning, we use the SCAND dataset [17], which contains 124 ROS bag recordings collected across diverse environments and conditions. We reserve 20% of the bags (25 recordings) as a held-out test set and use the remaining recordings for training and validation.

B. Policy Training Details

All policies were finetuned on $8 \times$ Nvidia A6000 GPUs using the augmented SCAND dataset mentioned in Sec. IV-A.

a) OmniVLA fine-tuning: We fine-tune OmniVLA (7.5B) [13] using LoRA [14] while keeping the backbone frozen. Gradient accumulation is used for 10 steps during fine-tuning, and training is initialized from the pretrained checkpoint released by the OmniVLA authors. All training hyperparameters are reported in Tab. IV.

Parameter	Value
Total steps	12,500
Batch size per GPU	4 (grad accum. 10)
Learning rate	1×10^{-4}
LR decay start	100,000 steps (10 \times drop)
Waypoints per sample	8
LoRA rank	32
Trainable weights	$\sim 3\%$ (adapters + heads)

TABLE IV: OmniVLA fine-tuning hyperparameters.

b) ViNT fine-tuning: We fine-tune ViNT [29] end-to-end on the CHOP training split using supervised imitation of human-preferred trajectories. Training is performed with a cosine learning rate schedule and a short warm-up period. All hyperparameters are summarized in Tab. V.

Setting	Value
Epochs	30
Batch size per GPU	1024
Learning rate	5×10^{-4}
Optimizer	AdamW
Scheduler	Cosine (warmup 4 epochs)
Context size	5 frames (temporal)
Predicted horizon	5 waypoints
Negative mining	5%

TABLE V: ViNT fine-tuning hyperparameters.

c) GNM fine-tuning: We fine-tune GNM [27] end-to-end on the same training split using supervised imitation of human-preferred trajectories. Training details and hyperparameters are provided in Tab. VI.

C. Offline Qualitative Results Analysis

Fig. 5 qualitatively compares baseline (blue) and CHOP-aligned (red) trajectory predictions for OmniVLA, GNM, and ViNT under the same observations and long-horizon goal.

In Scenario 1 (an indoor hallway with two pedestrians, one moving in the same direction as the robot and one moving in the opposite direction), the CHOP-aligned policies tend to plan

Parameter	Value
Epochs	40
Batch size per GPU	2048
Learning rate	7×10^{-4}
Optimizer	Adam
Context size	5 frames (temporal)
Predicted horizon	5 waypoints
Negative mining	5%

TABLE VI: GNM fine-tuning hyperparameters.

paths that bias toward wider lateral separation from pedestrian flow and exhibit more conservative progress in several frames, including pausing briefly (where no forward plan is rendered). The corresponding baselines more often plan paths that lie directly in the line of moving humans. The ViNT policy exhibits trajectories of highly varying quality. While some trajectories avoid the humans others appear to steer into them. This may help explain the inconsistent real-world results.

Scenario 2 shows an indoor lobby with static structure (walls and seating) and a pedestrian close to the robot’s right. Here, CHOP-aligned OmniVLA and GNM trajectories more consistently maintain a centered path and slow down, while baseline plans are more willing to track closer to both the chairs and the pedestrian.

Scenario 3 depicts a crowded outdoor walkway adjacent to a blue construction barrier on the right. In this scene, CHOP-aligned OmniVLA and GNM more frequently choose to laterally offset earlier and occasionally slow or stop as pedestrians pass, whereas baseline trajectories plan paths that directly run into pedestrians. Neither the baseline nor the fine-tuned ViNT policy consistently outperforms the other, and both occasionally plan trajectories that run into pedestrians.

For ViNT, the qualitative difference between baseline and CHOP-aligned predictions is less consistent across the three scenarios. In some frames, the CHOP-aligned path shifts laterally, but overall the red and blue plans often remain similar in shape and commitment. This trend remains consistent with the real-world demonstrations.

D. Distributions of Trajectory Metrics in Offline Dataset

Fig. 6 shows the full distributions of the test set for offline evaluation metrics for all three models before and after CHOP fine-tuning, complementing the mean results reported in Table II. Examining the distributions provides insight into how CHOP alters policy behavior beyond average performance.

Near-collision. Across all three architectures, CHOP fine-tuning produces a clear leftward shift in the near-collision distributions, indicating a systematic reduction in unsafe interactions. This effect is most pronounced for GNM and OmniVLA, where the finetuned distributions exhibit substantially reduced mass at higher near-collision values compared to their baselines. ViNT also shows a reduction in near-collision frequency, though the shift is less concentrated, consistent with its smaller gains in mean performance.

Deviation from preferred trajectories. Deviation distributions shift consistently toward lower values after CHOP

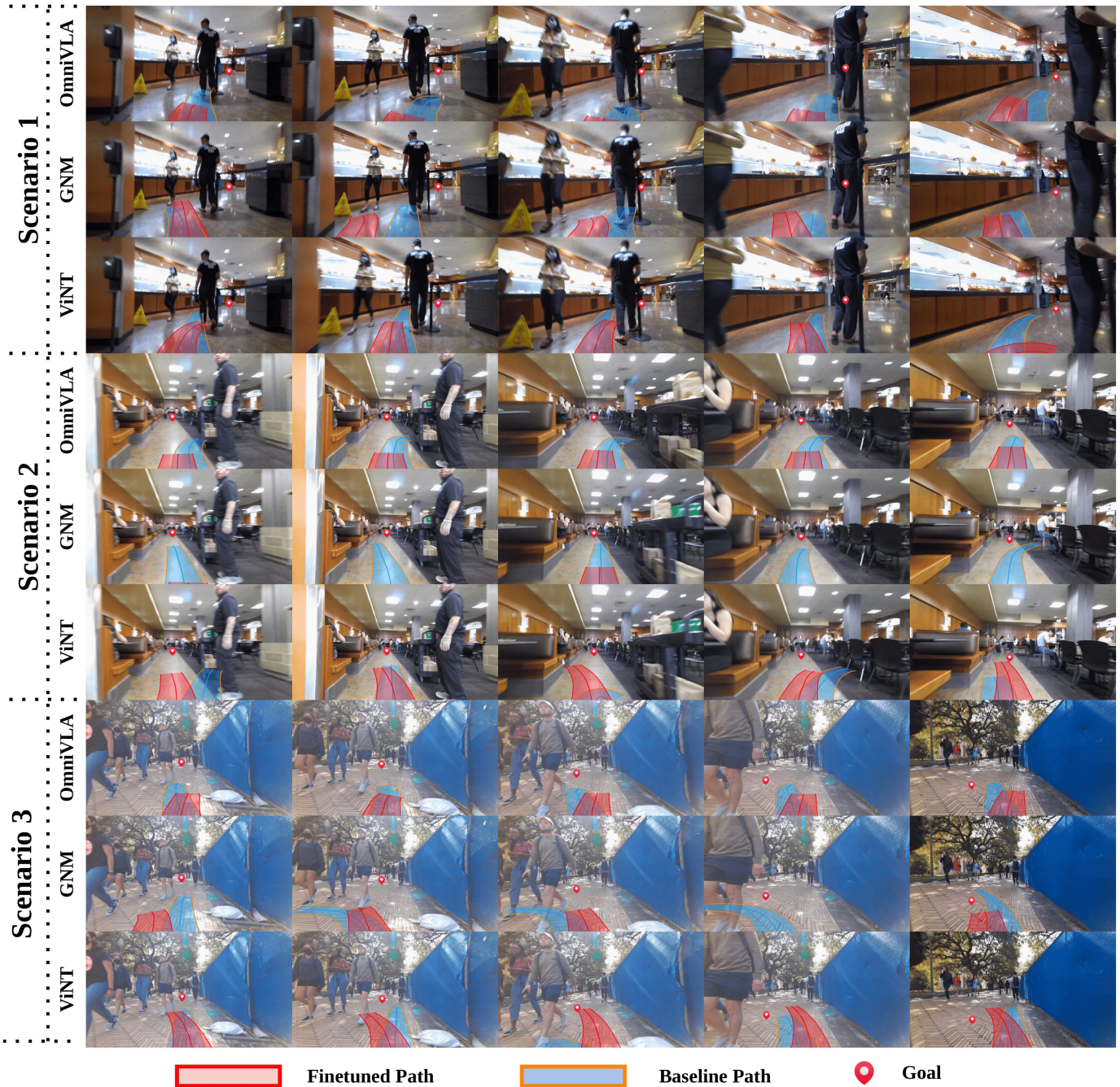


Fig. 5: Offline qualitative comparison on the SCAND test set showing successive frames (left to right) from three navigation scenarios. Each scenario is visualized across three rows corresponding to OmniVLA, GNM, and ViNT. Blue trajectories denote baseline model predictions, while red trajectories denote CHOP-aligned predictions. When a trajectory disappears from view, the policy has slowed or stopped due to conservative planning. Across most scenarios, timestamps, and methods, CHOP-aligned policies exhibit earlier obstacle avoidance, increased clearance, and more cautious behavior in the presence of dynamic agents compared to their baseline counterparts.

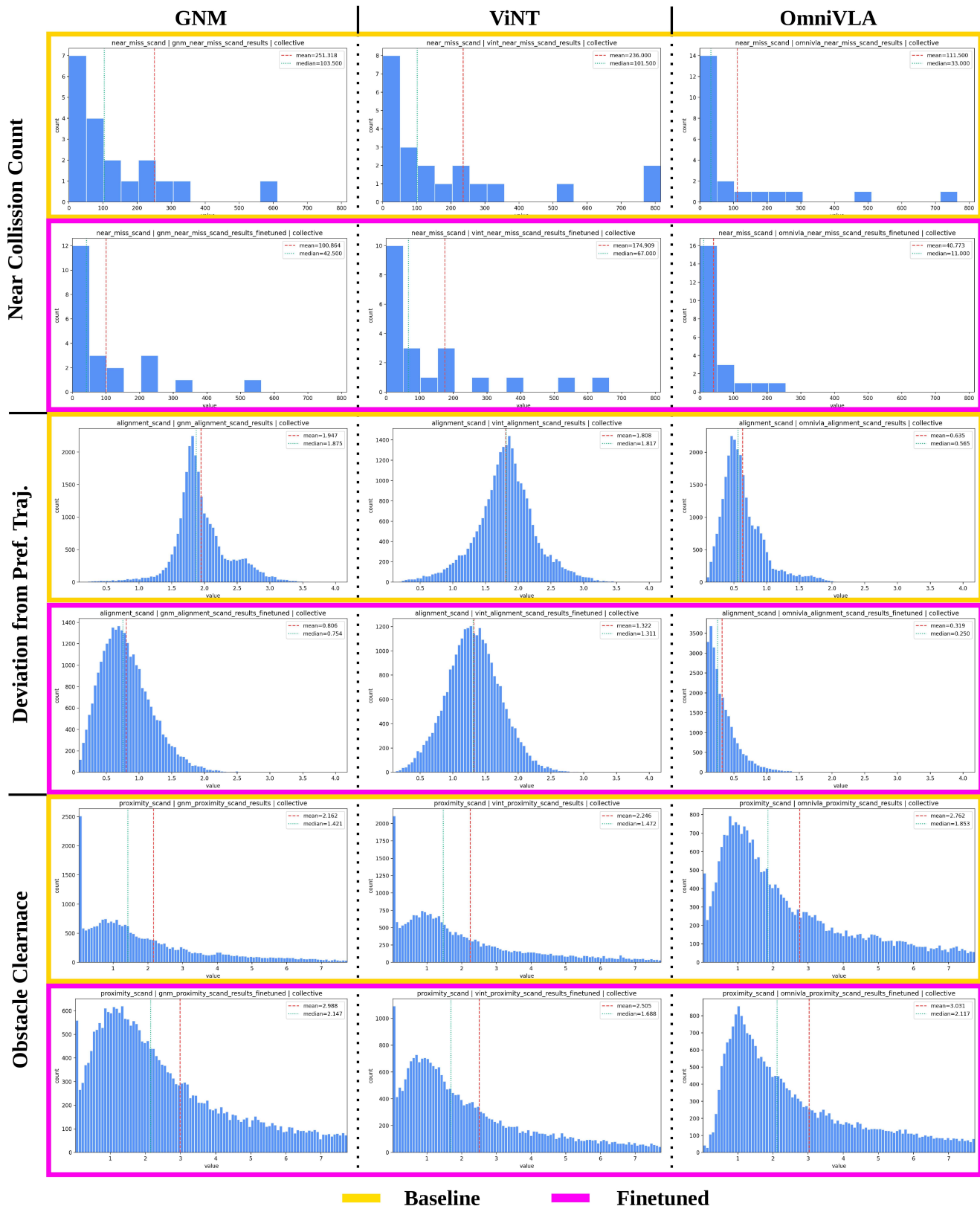


Fig. 6: Distribution of offline evaluation metrics on the SCAND test set for baseline (yellow) and CHOP-finetuned (pink) policies across GNM, ViNT, and OmniVLA. From top to bottom: near-collision count, deviation from human-preferred trajectories, and minimum obstacle clearance. CHOP fine-tuning shifts the distributions toward fewer near-collisions, lower deviation, and increased clearance, indicating improved safety and alignment beyond mean performance.

fine-tuning, demonstrating improved alignment with human-preferred trajectories. For GNM and OmniVLA, the finetuned distributions become both tighter and more centered around lower deviation values, suggesting not only better alignment on average but also reduced variance in behavior. ViNT exhibits a modest shift toward lower deviation values; however, the variance of the deviation distribution remains largely unchanged compared to the baseline.

Obstacle clearance. Obstacle clearance distributions shift rightward for all three models after CHOP fine-tuning, reflecting increased safety margins during navigation. GNM shows the largest distributional change, with a clear reduction in low-clearance trajectories and increased probability mass at higher clearances. OmniVLA similarly exhibits a rightward shift, while ViNT demonstrates a smaller but consistent improvement.

Overall, these distributional changes confirm that CHOP fine-tuning induces consistent, population-level behavior shifts rather than isolated improvements driven by outliers. The alignment gains, the reduction in unsafe behavior, and the increased obstacle clearance observed across the distributions mirror the trends in the aggregate metrics and validate counterfactual human preference supervision as an effective mechanism to improve safety-aware navigation.

E. Real-World Eval Analysis

The finetuned and baseline models are deployable on multiple robot platforms as the underlying trained models are robot agnostic. We test this on a Clearpath Robotics husky, and demonstrate better performance in the finetuned models. See video for more information.

F. Deployment Architecture

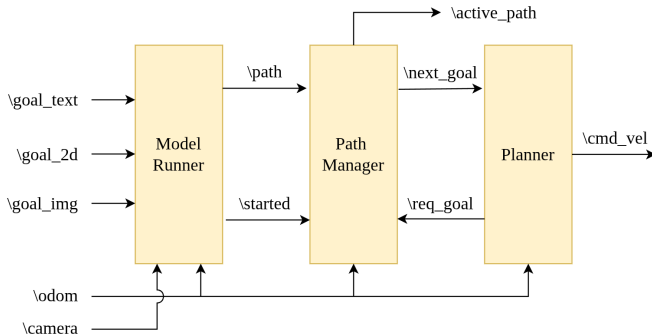


Fig. 7: ROS 2-based deployment architecture used for real-world execution. A model runner asynchronously produces short-horizon waypoint sequences, a path manager maintains and updates the active trajectory, and a planner tracks the current waypoint to generate velocity commands. The design decouples policy inference from low-level control and supports modular swapping of visuomotor policies.

To execute CHOP-aligned visuomotor policies on real robots, we employ a lightweight and modular execution architecture implemented in ROS 2. The system is composed of three independent nodes: a *model runner*, a *path manager*, and a low-level *planner*, as illustrated in Fig. 7. This design

explicitly decouples policy inference from trajectory execution, enabling robust operation under inference latency and supporting modular replacement of navigation policies.

The **model runner** node encapsulates the learned visuomotor policy. It consumes onboard sensor observations (RGB images and odometry) along with a goal specification (e.g., goal image, goal text, or 2D goal). Whenever computational resources are available, the model runner performs inference and publishes a short-horizon sequence of waypoints expressed in the robot’s local start frame on the `/path` topic, along with a `/started` signal indicating the availability of a new trajectory. Importantly, inference is performed asynchronously and is not tied to a fixed execution rate.

The **path manager** node subscribes to predicted waypoint sequences and maintains the most recent trajectory as the *active path*. When a new trajectory is received, a corresponding start signal (`/started`) is used to record the robot’s odometry pose at the time of planning. This stored start pose allows the path manager to consistently transform waypoints back into the frame in which the trajectory was generated and subsequently re-express them in the robot’s current odometry frame. At each control cycle, the path manager (i) removes waypoints that have already been traversed or lie behind the robot based on a fixed proximity threshold, (ii) publishes the first remaining waypoint as the current navigation target on `/next_goal`, and (iii) optionally republishes the trimmed trajectory on `/active_path` for visualization and monitoring. The path manager advances through the waypoint sequence until the path is exhausted or replaced by a new prediction.

The **planner** node subscribes to the current navigation target and generates low-level velocity commands (`/cmd_vel`) to track the provided waypoint. By operating on a single waypoint at a time, the planner remains agnostic to the length of the predicted trajectory and is compatible with any policy that outputs a sequence of waypoints.

This execution architecture provides several practical benefits. First, it enables continuous motion even under slow or variable inference times by reusing the most recent predicted trajectory while new predictions are computed. Second, continuous re-framing of waypoints into the current odometry frame improves robustness to execution drift and small localization errors. Third, automatic pruning of stale waypoints prevents oscillations and pursuit of outdated goals. Finally, because the planner and path manager operate purely on waypoint sequences, the execution stack is agnostic to the underlying policy and allows visuomotor models to be swapped or updated without modification to the downstream controller. Overall, this model-agnostic design allows CHOP-aligned policies to be deployed reliably on real robots.